Supporting Information

The Role of Structural Enthalpy in Spherical Nucleic Acid Hybridization

Lam-Kiu Fong,[1,6] Ziwei Wang,[2,6] George C. Schatz,[1,6] Erik Luijten,*[3,4,5] and Chad A. Mirkin*[1,3,6]

[1]Department of Chemistry, [2]Graduate Program in Applied Physics, [3]Department of Materials Science and Engineering, [4]Department of Physics and Astronomy, [5]Department of Engineering Sciences and Applied Mathematics, [6]International Institute for Nanotechnology, Northwestern University, Evanston, IL 60208, United States

*Corresponding authors

Table of Contents:

I. EXPERIMENTAL METHODS

Materials

The following chemicals were purchased and used as received. 5.9-nm gold nanoparticles were purchased from Ted Pella. Phosphoramidites were purchased from Glen Research. Dithiothreitol (DTT), sodium chloride (NaCl), sodium dodecyl sulfate (SDS), and Potassium Cyanide (KCN) were purchased from Sigma-Aldrich.

DNA Synthesis and Sequences

Oligonucleotides were synthesized using solid-phase phosphoramidite chemistry (MerMade-6, BioAutomation). Post synthesis, oligonucleotides were purified by reverse-phase high-performance liquid chromatography (RP-HPLC) on a Varian Microsorb C18 column (10 μm, 300×10 mm). The sequences used are listed below.

#	LABEL	SEQUENCE
1	12-mer Linear	5' TCCACTCATACT 3'
2	12-mer Linear Dabcyl	5' [DABCYL]TCCACTCATACT 3'
3	Complementary 12-mer	5' AGTATGAGTGGA 3'
4	Complementary 12-mer Dye	5' AGTATGAGTGGA [AF488] 3'
5	SNA_T_{10}12-mer	5' TCCACTCATACT(T_{10})-propylthiol-3'
6	SNA_T_{30}12-mer	5'-TCCACTCATACT(T_{30})-propylthiol-3'
7	SNA_T_{22}	5' TTTTTTTTTTTTTTTTTTTTTT-propylthiol-3'
8	12-mer Linear T_{10}	5' TCCACTCATACT(T_{10}) 3'

SNA Synthesis and Purification

Spherical nucleic acid gold nanoparticles (SNAs) were synthesized according to literature procedure.[1,2] Thiol-modified DNA (~0.13 μmols) was reduced with a 0.1 M solution of DTT for one hour. DTT was removed by size-exclusion chromatography with a NAP5 column (GE Healthcare). Purified DNA was then added to a solution of 5.9-nm gold nanoparticles (25 mL of ~83 nM) that was sonicated for 10 seconds and allowed to shake at 40°C for ~1 hr. For the next ~3 hours, 0.1 M sodium phosphate buffer (pH 7.4), 0.1% SDS, and 2 M NaCl, were added to the nanoparticle-DNA solution at 30-minute intervals followed by sonication and shaking. Once the DNA-nanoparticle solution reached a final concentration of 0.01 M sodium phosphate, 0.01% SDS and 0.5 M NaCl, it was shaken for 12–16 hours at 40°C. Following functionalization, excess DNA was removed from solution by centrifugation with > 50 kDa centrifugal filters (Amicon® Ultra-15). The SNAs were washed 3 times with 0.01% SDS and concentrated to a final volume of ~0.7 μL 0.01% SDS.

DNA Density Quantification on SNAs

The density of thiolated DNA on the surface of purified SNAs was determined by UV-Vis Spectroscopy (Cary 5000, Agilent). The concentration of nanoparticles and DNA was determined by the Beer–Lambert law ($A = \varepsilon bc$), which relates absorbance to concentration. For the gold nanoparticles, an extinction coefficient of $\varepsilon = 1.68E7$ ($M^{-1} \cdot cm^{-1}$) was used. To determine the concentration of DNA, the gold nanoparticle core was oxidatively dissolved by exposure to KCN (150mM final concentration). A DNA absorbance standard curve was created for each sequence, taking into consideration the KCN and SDS concentrations in the unknown SNA samples. DNA density measurements were performed in triplicate for each SNA sample.

Fluorescence Hybridization Experiments

Fluorescence hybridization experiments were performed on a Jobin Yvon Fluorolog FL3-22 spectrofluorometer over a temperature range of 55°C to 21°C. Fluorescence measurements were made at 2-degree increments with a 10-minute equilibration time at each point. Samples were prepared over a range of concentrations (2–20 nM) of either linear DNA with a quencher (sequence 2) or SNAs (sequence 5). For linear DNA experiments, (Alexa Fluor 488) dye-labeled complementary DNA (sequence 4) was added in a 1:1 DNA molar ratio. In the case of the SNA, the complementary strand was added in a 1:1 ratio of complement to nanoparticle. Experiments were performed in triplicate at each sample concentration.

Treatment of the SNA as a Single Entity for Analysis

This work treats the SNA as a single molecular entity rather than 46 individual DNA strands. This is the reason that in the van 't Hoff analysis the total concentration C_T is taken as the sum of complementary DNA strands plus SNAs, rather than the total DNA concentration.

The choice to treat the SNA as a single entity comes from applications, where the target complementary nucleic acid of interest is often present at substoichiometric concentrations relative to the SNAs. In this scenario, the binding constant of the first binding event on the SNA "molecule" determines its efficacy as a diagnostic and not the valency-corrected binding constant. Therefore, in the van 't Hoff analysis we consider the functional valency of the SNA (1:1 binding) rather than the structural valency.

Treatment of the SNA as 46 individual DNA strands in the van 't Hoff analysis would not consider negative cooperativity observed in this system, because any site on any SNA would be equally available for binding. At one extreme all strands on the SNA could be hybridized, which experiment shows does not occur due to each subsequent binding event being less favorable. Additionally, this treatment of the SNA as independent binding sites ignores the physical constraints placed on the DNA by covalently binding them to the nanoparticle. In this case, every DNA strand is able to freely explore the full volume of the container, which will have a large effect on the degrees of freedom of the system and greatly impact the entropy. In contrast, treatment of the SNA as a single molecule inherently captures the collective effect of interactions from neighboring strands on the first binding event (the nature of those interactions can then be discerned from simulation) and accounts for the restriction in degrees of freedom the DNA experiences from surface attachment. Therefore, treating the SNA as single polydentate molecule can more appropriately describe the first hybridization event.

Isothermal Titration Calorimetry Experiments

ITC experiments to measure DNA hybridization enthalpy directly were carried out on a MicroCal (GE Healthcare) ITC200 isothermal titration calorimeter at 25°C. ITC experiments measure heat released or absorbed during a reaction occurring at constant temperature.[3,4] In a typical experiment, complementary DNA strands are titrated into a sample cell containing DNA strands, either free in solution or radially oriented on the nanoparticles. Since DNA hybridization is an exothermic process, heat is released upon duplex formation, causing the sample cell temperature to increase. The heat required to maintain the temperature of the sample cell and a reference cell equal is monitored, allowing direct determination of hybridization enthalpy. Reaction stoichiometry is directly extracted from titration experiments if reactant concentrations are accurately known.

All samples including the reference buffer were prepared with Nanopure™ water (18.2 MΩ), 0.01% sodium dodecyl sulfate (SDS), and 0.3 M sodium chloride (NaCl). Titrant and sample cell concentrations were modified to both capture early hybridization events and ensure sample saturation. See tables below for sample concentrations. For each experiment, an initial 0.1-μL injection was performed to counteract autotitrator backlash. For linear DNA, ITC experiments consisted of 19 2-μL injections of complementary strand into 280 μL of linear strands. For SNAs, 57 0.7-μL injections of complementary strands were made.

Sample	Sequences	[Linear DNA] in Sample Cell	[Complementary DNA]
12-mer Linear	1,3	20 μM	200 μM

Sample	Sequences	[NP] in Sample Cell	[Complementary DNA]
SNA_T_{10}12-mer (high density)	3,5	0.714 μM	100 μM
SNA_T_{10}12-mer (low density)	3,5	1.0 μM	100 μM
SNA_T_{30}12-mer	3,6	0.714 μM	100 μM
SNA_T_{22}	3,7	0.714 μM	100 μM

II. COMPUTATIONAL METHODS

Simulation Model and Systems

We used the 3SPN.2 coarse-grained model,[5] which has been carefully parametrized to reproduce correct structural, thermodynamic, mechanical, and kinetic properties of DNA. This model separates the DNA into three sites per nucleotide, one each for the phosphate, sugar, and base. It has been implemented in the LAMMPS molecular dynamics package and is available for download.[6]

To simulate the SNA, the nanoparticle was modeled by a single bead, which interacts with all the DNA sites via a shift-truncated Lennard-Jones potential,

$$E_{NP\text{–site}}(r) = \begin{cases} 4\epsilon\left[\left(\frac{\sigma_{\text{NP–site}}}{r}\right)^{12} - \left(\frac{\sigma_{\text{NP–site}}}{r}\right)^{6} + \frac{1}{4}\right] & (r \le r_c) \\ 0 & (r > r_c) \end{cases},$$

where $\epsilon = 0.26$ kcal/mol and the cutoff distance $r_c = 2^{1/6}\sigma_{\text{NP–site}} = 3.2$ nm, which is the sum of the radius of the nanoparticle (3.0 nm) and the average radius of DNA sites (0.2 nm). The nanoparticle-bound DNA sequence with a 12-base "sticky end" and a poly-thymine linker region (T_{10} or T_{15}, sequence 5) and the complementary DNA (sequence 3) were designed to match experiment. To mimic the DNA density of experimental SNAs, 46 (high-density case) or 30 (low-density case) single-stranded DNA chains were grafted on the nanoparticle. The 3' end of the DNA was bonded on the nanoparticle surface using rigid-body dynamics. The grafted DNA strands were distributed uniformly on the sphere following a triangular pattern.

Implicit-Ion Simulations Method

Molecular dynamics (MD) simulations with implicit ions were performed to mimic experimental conditions for both the linear DNA system and the SNA system. For the SNA system, we simulated a single DNA-grafted nanoparticle in a cell of linear size 132.4 nm. This cell size yielded a nanoparticle concentration of 0.714 μM. In the linear DNA system, the number of DNA strands was set to either 30 or 46 in order to match the concentration in the SNA system. The cell size was chosen to be 135.6 nm and 156.3 nm, respectively, to maintain the linear DNA concentration at 20 μM. The concentration in both cases was consistent with experiments.

All simulations were performed in the *NVT* ensemble using a Langevin thermostat in a 3D periodic cubic cell. All simulations were performed at 310 K (see discussion below concerning the choice of the simulation temperature) and at 0.3 M ionic strength. The Debye–Hückel approximation was used to model the interaction between phosphate sites, which carry a charge of –0.6.[5] All systems were simulated with a 10-fs time step for 50 ns during equilibration and a 20-fs time step for 1 μs during production. Ten independent runs were conducted for each condition to obtain ensemble averages.

Melting Curve Calculated from Implicit-Ion Simulations

To test the ability of this implicit-ion DNA model to predict thermodynamic properties of the relevant DNA sequences at an ionic strength of 0.3 M, we performed separate simulations to determine the melting curve of a linear DNA system consisting of 46 single DNA strands (sequence 1) and 46 complementary strands (sequence 3) at a concentration of 20 μM (for either sequence 1 or 3). These simulations were started with 46 fully duplexed DNA strands and ran for 3 μs of equilibration followed by 1 μs of production with a 20-fs time step for both processes.

We note that the system reached equilibrium very quickly (within 50 ns) when the temperature was away from the melting temperature. Yet, we imposed the extended 3-μs equilibration period to guarantee equilibration at temperatures close to the melting temperature. The total number of complementary base pairs being formed $n_{\mathrm{bp}}$was calculated at each time step, and the average fraction of dehybridized base pairs was given by $(1-\frac{\langle n_{\mathrm{bp}}\rangle}{12\times 46})$, where the angular brackets denote the time average. This yields the computational melting curve:

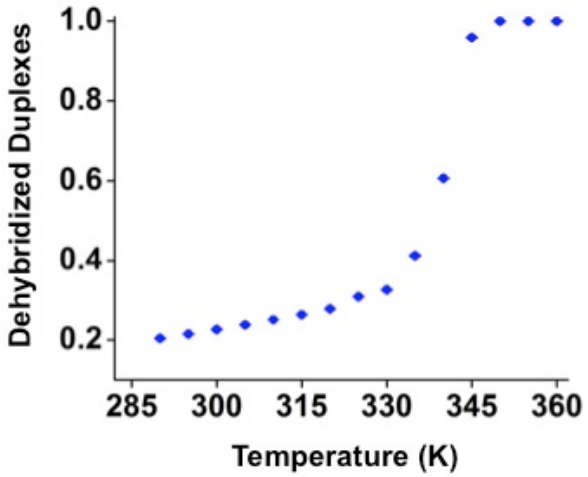

The maximum slope of the melting curve yields a melting temperature around 340 K. The predicted melting temperature for linear DNA of this sequence at 20 μM sample concentration and 0.3 M ionic strength is 326.4 K, as calculated using the OligoAnalyzer tool on the IDT website.[7] Thus, our implicit-ion DNA model gave a melting temperature that was 4% higher than the nearest-neighbor prediction from the OligoAnalyzer tool. This increase of the melting temperature at higher ionic strength has been attributed to the use of the Debye–Hückel approximation.[8] Because experiments were performed at room temperature (298 K), i.e., around 91% of the predicted melting temperature, we performed all implicit-ion simulations at 310 K (91% of the melting temperature of the simulation model) to make experiment and simulation comparable.

Calculation of Hybridization Enthalpy in Implicit-Ion Simulations

The hybridization enthalpy ΔH was calculated as the difference between the total energy of the system in the hybridized state (E_{H}) and the unhybridized state ($E_{\mathrm{U}} + E_{\mathrm{S}}$), as shown in Figure 2A of the main text. Specifically, for the unhybridized state of the linear DNA system, E_{U} is the total energy of 30 or 46 single strands of DNA (sequence 1), and E_{S} is the total energy of the complementary strand (sequence 3, box size 43.6 nm). To simulate the hybridized state, we replaced one single-stranded DNA in the multi-strand unhybridized system with a hybridized duplex (sequence 1 with sequence 3) and calculated the average total energy E_{H} after equilibration. Similarly, for the SNA system, the hybridized state refers to the system where one of the 30 or 46 grafted DNA chains has already formed a duplex with a complementary strand (sequence 3). The total energy of each state was obtained by taking the time average during each run and ensemble average over 10 independent runs.

Explicit-Ion Simulation Model and Procedure

MD simulations with explicit ions were also performed, both for the linear DNA system and for the SNA system. We again used the 3SPN.2 coarse-grained model, which has recently been extended to include explicit ions.[8] Enough positive counterions (Na^+) to compensate for the negatively charged phosphate sites on the DNA and 0.3 M NaCl salt were explicitly added to the system. Because the large number of ions significantly increased the simulation time, especially for large simulation cell sizes, we maintained the box size at 50 nm in both cases. For the SNA system, we simulated a single nanoparticle with 46 grafted DNA chains (linker region T_{10}), resulting in a nanoparticle concentration of 13.29 μM. For the linear DNA system, we included 10 DNA chains in the box, resulting in a DNA concentration of 132.85 μM.

All simulations were performed at 298 K (room temperature), with a 10-fs time step for 100 ns of equilibration and a 20-fs time step for 1 μs of production. Five independent runs were conducted to obtain an ensemble average. All other parameters were identical to those used in the implicit-ion simulations.

Calculation of Hybridization Enthalpy in Explicit-Ion Simulations

The hybridization enthalpy ΔH in the explicit-ion simulations was calculated as the difference between the total energy of the system in the hybridized state (E_H) and the unhybridized state (E_U). In contrast to the implicit-ion simulations, we did not take into account the total energy of a single complementary target (E_S) when determining the unhybridized state. We reasoned that since E_S contains the ion–ion interaction energy it should not be added to E_U. Since the same E_S applies to the SNA hybridization and the free DNA hybridization, this choice has no effect on the calculation of the *difference* in hybridization enthalpy, $\Delta\Delta H$, but it does affect the quoted values for the hybridization enthalpies themselves.

For the unhybridized state of the linear DNA system, E_U is the total energy of 46 single strands of DNA (sequence 1). To simulate the hybridized state, we replaced one single-stranded DNA in the unhybridized system with a hybridized duplex (sequence 1 with sequence 3) and calculated the total energy E_H after equilibration. Similarly, for the SNA system, the hybridized state refers to the system where one of the 46 grafted DNA chains has already formed a duplex with a complementary target (sequence 3). The total energy of each state was obtained by taking a time average for each run and an ensemble average from five independent runs.

III. CONCENTRATION-DEPENDENT MELTING STUDIES

Figure S1: To confirm that the van 't Hoff analysis reflects thermodynamic equilibrium values, we verified the absence of hysteresis between hybridization and dehybridization at the lowest sample concentrations (1 nM complementary DNA) for (A) 1 nM linear DNA and (B) 1 nM SNAs.

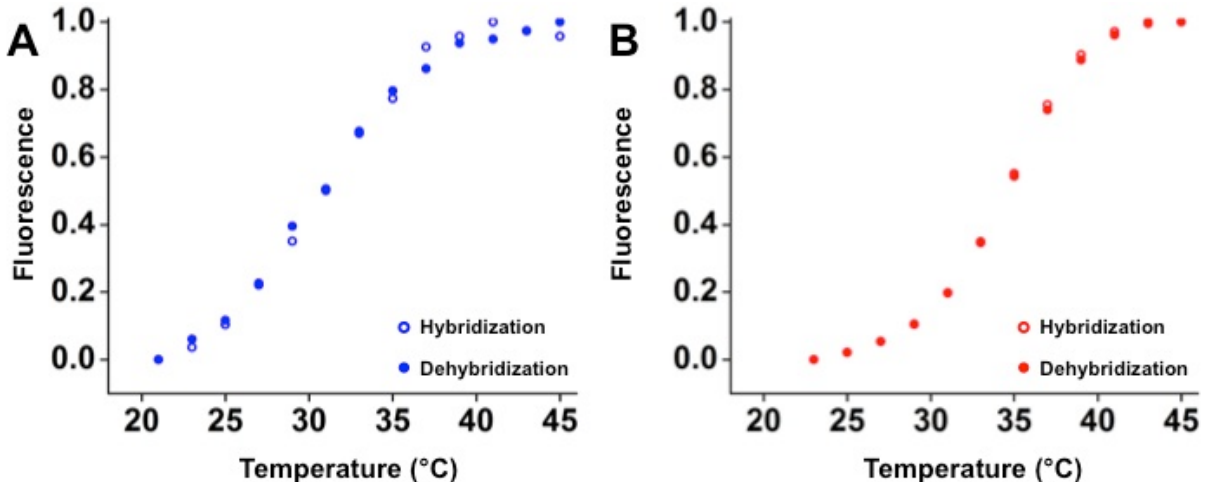

Figure S2: Concentration dependence of the helix–coil transition temperature for (A) linear DNA hybridization and (B) SNA hybridization.

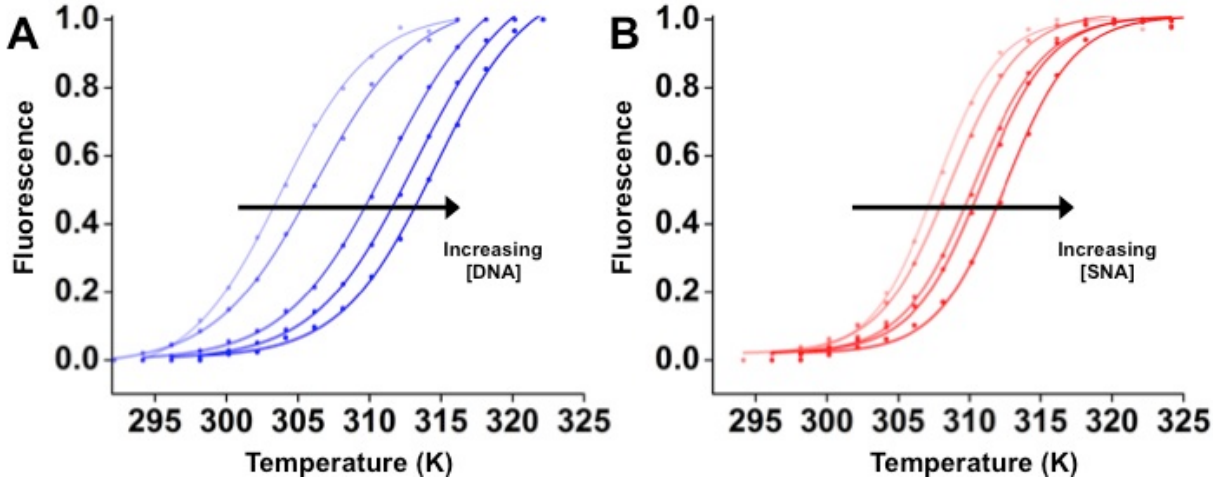

Table S1: Thermodynamic constants derived from the van 't Hoff analysis.

Thermodynamic Constant	Linear DNA	SNA
$\Delta H°$ (kcal/mol)	–40.6 ± 2.4	–91.3 ± 5.5
$T\Delta S°$ (kcal/mol)	–27.2 ± 2.3	–75.8 ± 5.3
$\Delta G°$ (kcal/mol) at 298 K	–13.4 ± 0.1	–15.5 ± 0.2
K_{eq} (M^{-1}) at 298K	$6.8\times10^{9} \pm 1.1\times10^{9}$	$2.3\times10^{11} \pm 8.5\times10^{10}$

IV. ISOTHERMAL TITRATION CALORIMETRY EXPERIMENTS

Figure S3: To confirm that the heats observed in the calorimetric measurements were strictly the result of duplex formation, control experiments were performed to rule out other enthalpic contributions. Shown in black are (A) the heat of complementary DNA dilution, determined by titrating complementary DNA (sequence 3) into buffer (0.01% SDS, 0.3 M NaCl) and (B) the heat of complementary DNA association with a non-binding SNA, determined by titrating complementary DNA (sequence 3) into a solution containing SNAs functionalized with 45 non-complementary DNA strands (sequence 7). Raw power data for linear DNA hybridization is provided in blue for comparison in each case.

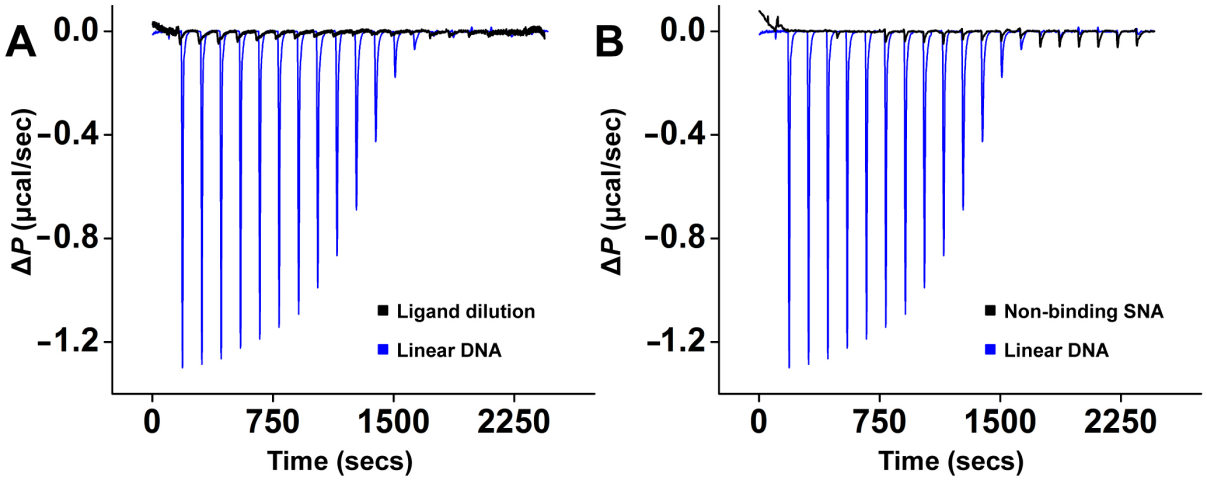

Figure S4: To determine the contribution of the T_{10} linker region to linear strand hybridization, the heat of complementary strand association with a linear 12-mer T_{10} (sequence 8) was measured. (A) Comparison of ITC data and (B) break-down of enthalpic and entropic contributions for the linear 12-mer (blue) and the linear 12-mer T_{10} (black). See Table S2 for values. A: Upper panels: differential heating power ΔP *vs*. time; lower panels: integrated heats of reaction Q *vs*. molar ratio.

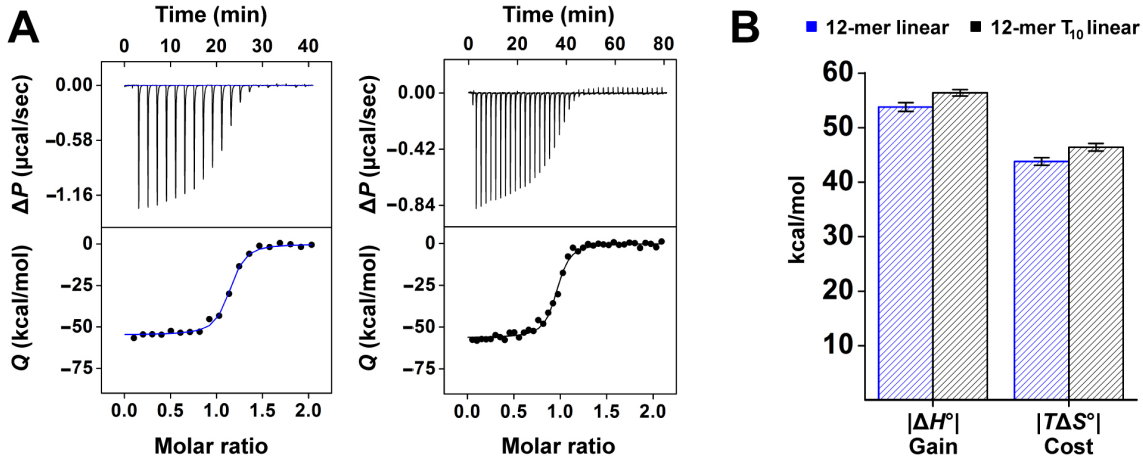

Figure S5: To examine the effect of nearest-neighbor binding contributions on the measured enthalpy of complement hybridization on SNAs, the number of binding sites on the surface was decreased while maintaining the same density of DNA strands (~45 strands/particle). This was achieved by introducing a non-binding filler strand of the same length (sequence 7). SNAs were functionalized with either (A) 25:75 binding to non-binding DNA or (B) 50:50 binding to non-binding DNA. (C) Hybridization enthalpy of the first few binding events plotted as a function of percentage of binding strands on the SNA. The enthalpies of a completely binding SNA (100%) and a completely non-binding SNA (0%), as well as the enthalpy of linear strand hybridization are provided for reference. This demonstrates that the enthalpy of hybridization for the first few strands on SNAs does not depend on the ability of neighboring single strands to form productive duplexes. An enhancement in the hybridization enthalpy on SNAs relative to linear DNA was solely a consequence of the surface density of DNA. (A,B): Upper panels: differential heating power ΔP *vs*. time; lower panels: integrated heats of reaction Q *vs*. molar ratio.

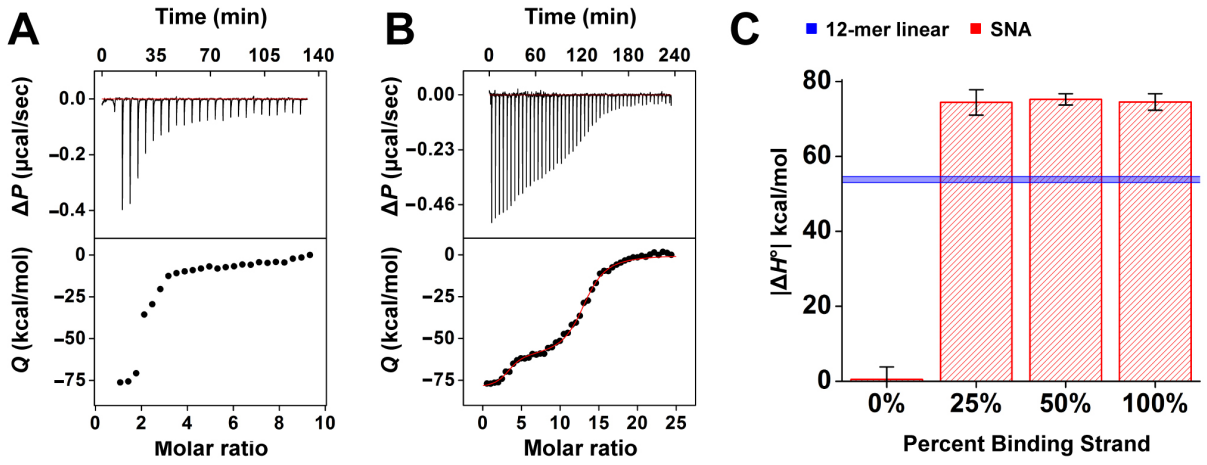

Figure S6: ITC of (A) low-density SNAs (~30 strands per particle) and (B) SNAs functionalized with 45 strands of longer, more flexible 12-mer T_{30} linker DNA (sequence 6). Upper panels: differential heating power ΔP *vs*. time, lower panels; integrated heats of reaction Q *vs*. molar ratio.

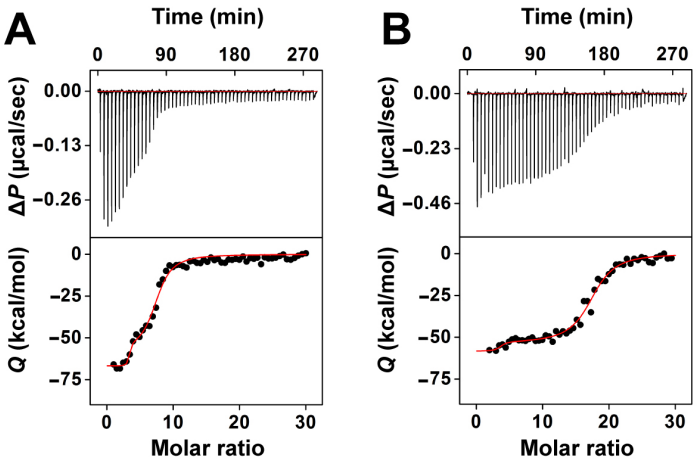

Table S2: ITC-derived enthalpies were obtained by direct integration of power (ΔP) *vs.* time peaks to ensure that the values were model independent. For further analysis, the ITC data was fitted to either a one-site binding model (in the case of linear DNA) or a two-site binding model (in the case of SNAs). A two-site binding model for SNAs was based purely on the shape of the calorimetrically derived isotherm, which has two inflection points. This type of fitting allowed extraction of model-dependent thermodynamic constants ($\Delta S°$, K_{eq}). Data for both types of binding sites on the SNA are listed consecutively when applicable. SNA sample names are listed based on the sequence of DNA used (see the methods section for a list of sequences). Labels "High" and "Low" refer to high and low density of DNA on the nanoparticles, respectively.

Sample	Loading	*N* (Stoichiometry)	$\Delta H°$ (kcal/mol)	$\Delta S°$ (kcal/mol *K)	K_{eq} (M^{-1})
SNA_T_{10}12-mer (High)	46 ± 1	4	–74.5 ± 2.1	–0.207 ± 0.009	$2.58\times10^{9} \pm 2.73\times10^{9}$
		15	–54.5 ± 1.5	–0.152 ± 0.005	$6.03\times10^{6} \pm 1.79\times10^{6}$
SNA_T_{10}12-mer (Low)	30± 1	3	–68.1 ± 1.7	–0.181 ± 0.005	$2.39\times10^{9} \pm 6.94\times10^{9}$
		4	–57.9 ± 3.5	–0.164 ± 0.006	$6.82\times10^{6} \pm 9.09\times10^{5}$
SNA_T_{30}12-mer	45 ± 1	3	–58.5 ± 1.9	–0.152 ± 0.008	$5.05\times10^{8} \pm 4.68\times10^{8}$
		14	–53.0 ± 4.7	–0.147 ± 0.016	$5.08\times10^{6} \pm 1.34\times10^{6}$
SNA_T_{22}	51 ± 1	N/A	–4.6 ± 1.6	N/A	N/A
SNA_T_{10}12-merT_{22}_5050	53 ± 1	3	–75.1 ± 1.5	–0.229 ± 0.005	$2.24\times10^{8} \pm 1.15\times10^{8}$
SNA_T_{10}12-merT_{22}_2525	48 ± 1	3	–74.3 ± 3.4	N/A	N/A
Linear 12-mer	N/A	1	–53.8 ± 0.8	–0.147 ± 0.003	$2.05\times10^{7} \pm 5.62\times10^{6}$
Linear 12-mer T_{10}	N/A	1	–56.4 ± 0.6	–0.155 ± 0.004	$1.94\times10^{7} \pm 3.03\times10^{6}$

V. FURTHER DISCUSSION OF COMPUTATIONAL RESULTS

Table S3: Break-down of energy contributions to the enthalpy of hybridization obtained from implicit-ion simulations for linear 12-mer DNA (sequence 1) and an SNA functionalized with 46 single strands of the same 12-base sequence with a T_{10} single-stranded linker region (sequence 5). The largest contribution to the enthalpy difference between linear and SNA hybridization is the structural energy, which is composed of bond, angle, dihedral, and intra-strand base-stacking energies. There are small contributions from base pairing (BP), cross-stacking (CS) between strands, and Coulombic interactions. The change in the number of base pairs formed (Δn_{bp}) in each case is provided for reference, to demonstrate that Watson–Crick base pairing is nearly identical in both cases.

Sample	ΔH (kcal/mol)	ΔE (Structural)	ΔE (BP)	ΔE (CS)	ΔE (Coulomb)	Δn_{bp}
Linear	–86.13 ± 0.54	–34.04 ± 0.62	–44.03 ± 0.04	–8.76 ± 0.01	0.48 ± 0.01	8.97 ± 0.09
SNA	–91.41± 1.64	–38.37 ± 1.70	–44.78 ± 0.07	–9.07 ± 0.02	0.81 ± 0.10	9.14 ± 0.14

Figure S7: Comparison of the structural energy obtained from implicit-ion simulations of the nanoparticle-attached DNA strand before and after hybridization. The strand region for which the structural energy was calculated is enclosed in a purple dashed box. (A) Comparison of the change in structural energy (ΔE) due to hybridization for the linear and the SNA duplexes showed no difference within error. (B) The T_{10} single-stranded linker region that associates the duplex binding region to the nanoparticle became more ordered and therefore structurally stabilized by ~0.6 kcal/mol after hybridization, as shown by a difference in the structural energy (E) before and after hybridization. (C) The entire nanoparticle-bound strand experienced a hybridization-induced structural stabilization ~2.2 kcal/mol greater than the stabilization observed in the linear case. If the stabilization experienced by the T_{10} region is subtracted, the remaining ~1.6 kcal/mol must have originated from the structural stabilization (more energetically favorable angles, dihedrals, and base stacking) of the DNA junction region, which connects the duplex to the T_{10} linker. All energies are given in units of kcal/mol.

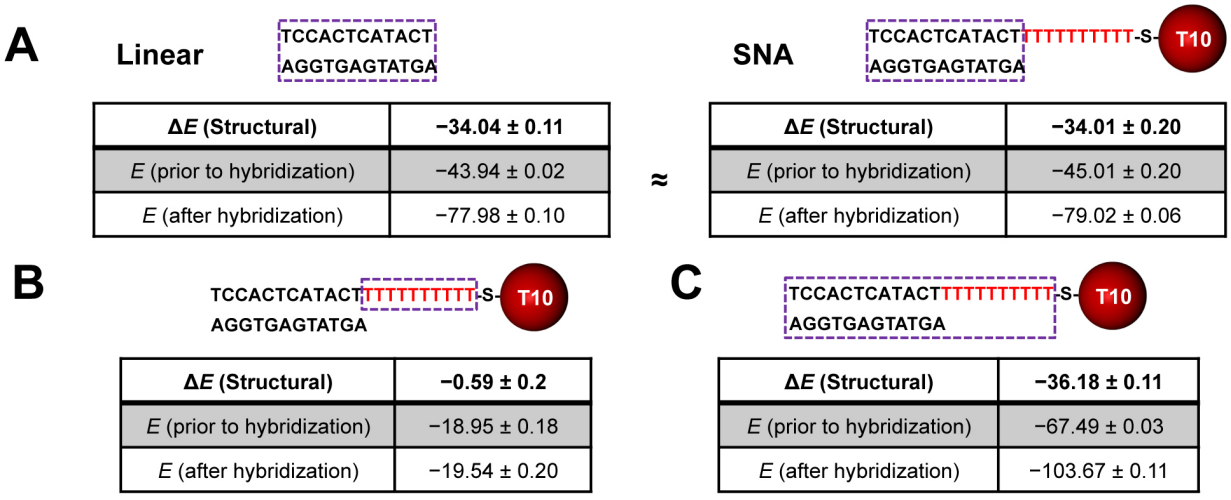

Figure S8: Comparison of hybridization enthalpies obtained from implicit-ion simulations for SNAs functionalized with different DNA (A) densities (High: 46 strands per particle, Low: 30 strands per particle) at fixed linker length (T_{10}) and (B) linker lengths (T_{10}: sequence 5, T_{15}: 5'-TCCACTCATACT(T_{15})-propylthiol-3') at a constant density of 46 strands per particle. (The enthalpy of linear DNA hybridization is provided in blue for reference.)

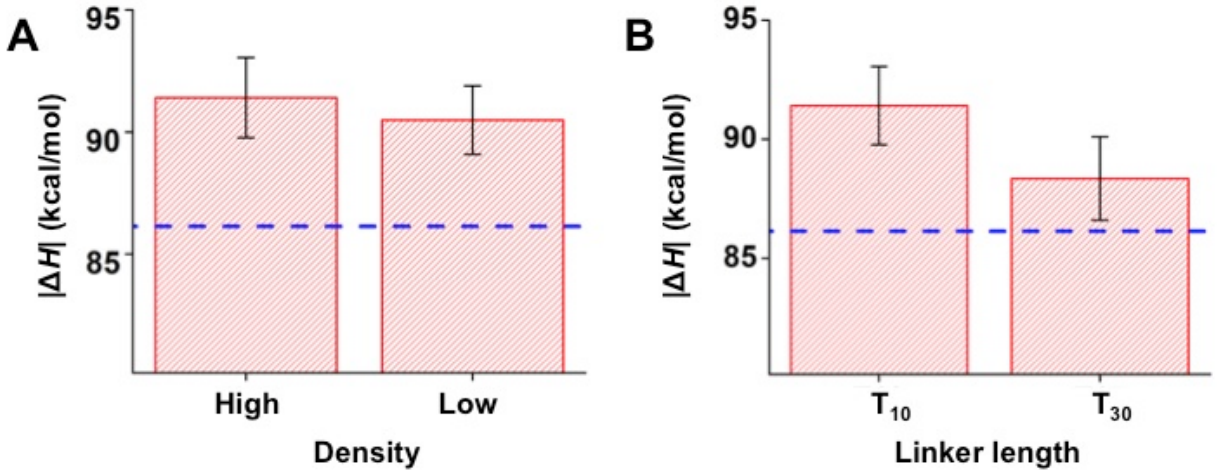

Figure S9: Comparison of the total structural energy obtained from implicit-ion simulations of the remaining 45 unhybridized nanoparticle-bound DNA strands before and after hybridization of a complement. The total structural energy of the remaining DNA strands became more favorable after hybridization by ~2 kcal/mol. This implies that all single-stranded DNA on the nanoparticle surface explored less unfavorable conformations after hybridization of one complement. When this stabilization energy is divided by the 45 strands on the nanoparticle surface, the effect per strand is very small. However, the sum of the contributions from individual strands has a significant effect on the overall structural energy of the system. This observation can help explain the significant entropic loss observed after DNA hybridization on SNAs. All strands, not merely the hybridizing strand, lose some degrees of freedom after hybridization.

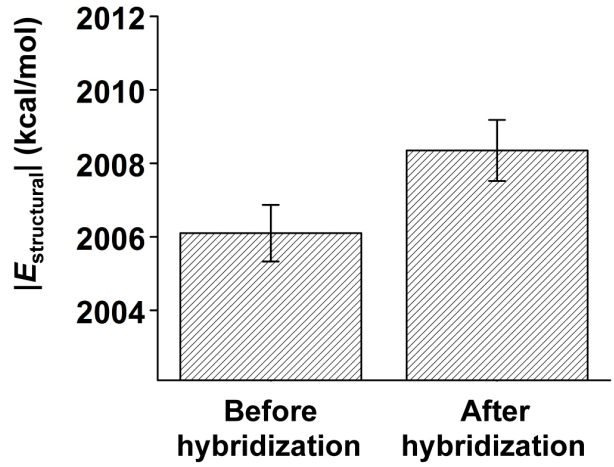

Condition	$E_{structural}$/Strand
Before hybridization	−44.58 ± 0.02
After hybridization	−44.63 ± 0.02

Table S4: Break-down of energy contributions to the enthalpy of hybridization obtained from explicit-ion simulations for linear 12-mer DNA (sequence 1) and an SNA functionalized with 46 single strands of the same 12-base sequence with a T_{10} single-stranded linker region (sequence 5). The results provided here are qualitatively the same as the implicit-ion results, confirming that the intra-strand structural energy is the largest contribution to difference in hybridization enthalpy.

Sample	ΔH (kcal/mol)	ΔE (Structural)	ΔE (BP)	ΔE (CS)	ΔE (Coulomb)	Δn_{bp}
Linear	–79.40 ± 1.03	–55.86 ± 0.34	–45.27 ± 0.02	–8.96 ± 0.01	–9.89 ± 0.37	9.35 ± 0.01
SNA	–84.70 ± 1.34	–60.37 ± 1.81	–45.85 ± 0.05	–9.25 ± 0.01	–9.81 ± 0.44	9.50 ± 0.01

VI. REFERENCES

(1) Hurst, S. J.; Lytton-Jean, A. K. R.; Mirkin, C. A. Maximizing DNA Loading on a Range of Gold Nanoparticle Sizes. *Anal. Chem.* **2006**, *78* (24), 8313–8318.

(2) Hill, H. D.; Millstone, J. E.; Banholzer, M. J.; Mirkin, C. A. The Role Radius of Curvature Plays in Thiolated Oligonucleotide Loading on Gold Nanoparticles. *ACS Nano* **2009**, *3* (2), 418–424.

(3) Freire, E.; Mayorga, O. L.; Straume, M. Isothermal Titration Calorimetry. *Anal. Chem.* **1990**, *62* (18), 950A–959A.

(4) Jelesarov, I.; Bosshard, H. R. Isothermal Titration Calorimetry and Differential Scanning Calorimetry as Complementary Tools to Investigate the Energetics of Biomolecular Recognition. *J. Mol. Recognit. JMR* **1999**, *12* (1), 3–18.

(5) Hinckley, D. M.; Freeman, G. S.; Whitmer, J. K.; de Pablo, J. J. An Experimentally-Informed Coarse-Grained 3-Site-Per-Nucleotide Model of DNA: Structure, Thermodynamics, and Dynamics of Hybridization. *J. Chem. Phys.* **2013**, *139* (14), 144903.

(6) 3SPN.2. https://uchic.ag/3spn2 (Accessed June 25, 2017).

(7) IDT OligoAnalyzer. https://www.idtdna.com/calc/analyzer (Accessed December 21, 2017).

(8) Hinckley, D. M.; de Pablo, J. J. Coarse-Grained Ions for Nucleic Acid Modeling. *J. Chem. Theory Comput.* **2015**, *11* (11), 5436–5446.